

*The International
C.S.R.*

Dynamics of **Continuous, Discrete & Impulsive** **Systems**

Editor-in-Chief
Xinzhi Liu, University of Waterloo

Published as an added volume to DCDIS series B:
Applications and Algorithms, ISSN 1492-8760

2005

Watam Press · Waterloo

Three-dimensional Mathematical Models of Phase Transformation Kinetics in Shape Memory Alloys

D. Roy Mahapatra

MMCS, Wilfrid Laurier University

75 University Avenue West, Waterloo, ON, N2L 3C5

droymahapatra@wlu.ca

R.V.N. Melnik

MMCS, Wilfrid Laurier University

75 University Avenue West, Waterloo, ON, N2L 3C5

rmelnik@wlu.ca

We develop a 3D mathematical model based on a fully coupled free energy representation of multi-variant martensitic phase transformations and discuss its computational implementation. In particular, we derive a finite element model by using variational minimization involving (1) momentum conservation (2) heat conduction with convective terms but dominated by stress-driven dissipation, and (3) first-order phase kinetics. We provide numerical results on the simulation of transient stress-driven phase field evolution in a NiAl thin film.

I. INTRODUCTION

Shape memory alloys (SMAs) in various forms and compositions have been successfully employed in many engineering applications. In recent years, a significant amount of research effort has been devoted to experimental characterization of new SMAs, increasingly through computational simulations. Controlled experiments on SMAs often become extremely complex because one has to deal with spatio-temporal control of deformation, stress and temperature. On the other hand, appropriate large-scale computational simulations with physically consistent mathematical models (see e.g. [1, 2, 3, 4, 5, 6, 7]) can address many important issues. However, results on the three-dimensional time-dependent dynamics of real-scale SMA devices are very limited. The objective of the research reported in this paper is to address some of the complex modeling issues and preliminary computer simulations based on a newly developed finite element model.

One of the crucial issues in numerical simulation for the problem under consideration is the accurate representation of the multi-variant Phase Transformation (PT). Phenomenological framework based on Landau theory of martensitic transformations is regarded as a basic building block. However, most of the phenomenological models are applicable at macroscopic and mesoscopic scales as discussed in [6]. A macroscopic model requires the description of the 3D geometry and variational minimization of an appropriate potential involving the thermoelastic energy and the energy due to dynamic self-accommodation of the martensitic variants. Whereas a mesoscopic model, such as the Falk-Konopka free energy model [8], requires the description of the free energy as a function of the strain invariants of a single crystal and its point group sym-

metry. Among earlier important developments, we note works by Ball and Cartensen [1] on the mechanism of self-accommodation process of the phases, results on experimental correlation, as well as a number of results on numerical simulations of (see e.g. [2, 9, 10, 11]). The present challenges in mathematical modeling and computational simulation of PT in shape memory alloys lie in the following: (1) enforcing adequate consistency conditions for three-dimensional thermo-elastically coupled situations and retaining the essential features of multi-variant transformation properties (2) incorporating such model into a finite element like variational framework (3) performing high-performance numerical simulation with adequate flow of physical information between the microstructural scale and the macroscopic scale.

In the present paper we implement a consistent microscopic free energy function [12] and the associated coupled field model in a three-dimensional finite element model. The description of the austenite and martensites in such free energy model (known as Gibbs free energy model) is represented by the order parameters (η_k). Such order parameters follow the important crystallographic compatibility properties, such as group symmetry, invariance, and most importantly, the minimum free energy state (quasi-static situation). Details on this can be found in [13, 14]. Further, the evolution of these ordered states are governed by a first-order kinetics, generally known as the time-dependent Ginzburg-Landau equation [4, 15]. However, in order to complete the description of such models, the value of spontaneous strain and certain material parameters are to be estimated from a molecular dynamic simulation. This was done in [14] by assuming a time-independent thermo-elastically decoupled case. The idea behind this is to obtain, on the one hand, the atomistic calculation of the free energy based on Born-Oppenheimer approximation, and on the other hand, to express this free energy in terms of the deformation gradient and temperature according to the Cauchy-Born rule. The order parameter (η_k) therefore describes the phenomenological link between the above two dynamics. This approach deviates from the notion of phase fractions [16, 17] and gives a consistent framework for microstructure evolution in multivariant situations. Given the problem complexity, it should be noted that up to date, no robust mathematical model and well-defined computational steps have been reported in the literature that can deal with general time-dependent dynamics of SMA over a range of

deformation, stress and temperature. However, rigorous analytical results on the stability and bounds on the numerical process of energy minimization have been obtained recently (e.g. Li and Luskin [18], Matus *et al.* [19]).

II. 3D LANDAU THEORY OF MARTENSITIC PHASE TRANSFORMATIONS

It has been demonstrated by Levitas and Preston [13, 4] that the polynomial structures 2-3-4 and 2-4-6 of the Gibbs free energy in order parameter η in Cartesian coordinates can eliminate the problem of unphysical minima and retain all the necessary properties of the Ginzburg-Landau free energy function with respect to point group symmetry of the crystals. Such polynomial structures can be made in such a way that the stability of the austenitic phase (A) and martensitic variants (M_j), non-extremal diffusion barrier and nucleation can be described in stress-temperature space. Furthermore, while using such a polynomial structure, the interfaces (domain walls) $M_j - M_i$ between the martensitic variants (i, j) can be interpreted by using a newly introduced barrierless A nucleation mechanism, i.e. by splitting the original into two simultaneously present interfaces $M_j - A$ and $A - M_i$. In this section a 2-3-4 polynomial structure is constructed by improving upon the model of Levitas and Preston [13, 14]. Below we briefly describe the Gibbs free energy representation for our model. The details are given in [12].

As a starting point of our consideration, let us consider a single variant of martensite and single order parameter $\eta \in [0, 1]$. First we define the Gibbs free energy density in stress-temperature space (σ, θ) as

$$G = -\sigma : \lambda : \sigma / 2 - \sigma : \varepsilon_t \varphi(\eta) + f(\theta, \eta), \quad (1)$$

where λ is the constant fourth-rank elastic compliance tensor, ε_t is the transformation strain tensor at the thermodynamic equilibrium of the martensite (obtained from crystallography), $\varphi(\eta)$ is a monotonic function with $\varphi(0) = 0$ indicating stable A phase and $\varphi(1) = 1$ indicating stable M phase. $f(\theta, \eta)$ is the chemical part of the energy with property: $f(\theta, 1) - f(\theta, 0) = \Delta G^\theta(\theta)$, where ΔG^θ is the difference between the thermal parts of the Gibbs free energy density of the M and A phases, which can be obtained indirectly from experiments through the relation [20]

$$\Delta G^\theta = -\Delta s_e(\theta - \theta_e) - \Delta c\theta [\ln(\theta/\theta_e) - 1] - \Delta c\theta_e, \quad (2)$$

where Δc is the difference between the specific heat of the phases, Δs_e is the jump in the specific entropy at the equilibrium temperature (θ_e). The objective is to obtain the functions φ and f by satisfying their properties mentioned above and the conditions of extremum of the energy for existence of equilibrium of A and M phases: $\partial G / \partial \eta = 0$ at $\eta = 0, 1$. Thus main step in the subsequent formulation that follows [12] is to assume the extremum in the form

$$\frac{\partial G}{\partial \eta} = \eta(\eta - 1)(\eta - \eta_b), \quad (3)$$

so that the roots $\eta = 0, 1$ correspond to the extrema and the root $\eta = \eta_b(\sigma, \theta)$ represents the $A \leftrightarrow M$ PT barrier.

Integrating Eq. (3) and imposing the combined properties of $\varphi(\eta)$ and $f(\theta, \eta)$ stated earlier as

$$G(\sigma, \theta, 0) - G(\sigma, \theta, 1) = \sigma : \varepsilon_t - \Delta G^\theta, \quad (4)$$

we get

$$\eta_b = -6\sigma : \varepsilon_t + 6\Delta G^\theta + 1/2. \quad (5)$$

After some algebraic steps, we explicitly obtain the polynomial structure in $\varphi(\eta)$ and then $f(\theta, \eta)$. For $A \rightarrow M$ PT, the criteria for the loss of stability of A phase is $\partial^2 G / \partial \eta^2 \leq 0$ at $\eta = 0$. Similarly, for $M \rightarrow A$ PT, the criteria for the loss of stability is $\partial^2 G / \partial \eta^2 \leq 0$ at $\eta = 1$. In the next section we describe how this procedure is extended to the multivariant case.

III. MULTIVARIANT PHASE TRANSFORMATION

In order to model macroscopic sample of SMA in realistic situations, it is essential to incorporate the effects of (1) martensitic variants (M_k) (2) thermal strain (3) unequal compliances across the interfaces and the resulting inhomogeneity. In this paper we consider cubic-to-tetragonal transformations. In this case, there are three variants of martensite according to the point group of crystallographic symmetry. The Gibbs free energy density thus should poses the associated invariance properties. In the mathematical model, this can be cross-checked by interchanging the variant indices (k). We assume the same order of variation in the compliance tensor and the thermal expansion tensor as in $\varphi(\eta)$. The Gibbs free energy density for cubic-tetragonal transformation having three variants $k = 1, 2, 3$ is expressed as

$$\begin{aligned} G = & -\sigma : \left[\lambda_0 + \sum_{k=1}^3 (\lambda_k - \lambda_0) \varphi(\eta_k) \right] : \sigma / 2 \\ & - \sigma : \sum_{k=1}^3 \varepsilon_{tk} \varphi(\eta_k) - \sigma : \left[\varepsilon_{\theta 0} + \sum_{k=1}^3 (\varepsilon_{\theta k} - \varepsilon_{\theta 0}) \varphi(\eta_k) \right] \\ & + \sum_{k=1}^3 f(\theta, \eta_k) + \sum_{i=1}^2 \sum_{j=i+1}^3 F_{ij}(\eta_i, \eta_j), \end{aligned} \quad (6)$$

where λ is the second-order forth-rank compliance tensor (λ_0 is for A phase), $\varepsilon_{\theta 0} = \alpha_0(\theta - \theta_e)$, $\varepsilon_{\theta k} = \alpha_k(\theta - \theta_e)$, α_0 and α_k are the thermal expansion tensor of A and M_k . F_{ij} is an interaction potential required to preserve the invariance of G with respect to the point group of symmetry and uniqueness of the multivariant PT at a given material point. The description of PT can now be generalized with three sets of order parameters: $\bar{0} = \{0, \eta_k = 0, 0\}$, $\bar{1} = \{0, \eta_k = 1, 0\}$ and $\bar{\eta}_k = \{0, \eta_k, 0\}$. The extremum property of the free energy density requires

$$\frac{\partial G}{\partial \eta_k} = \eta_k(\eta_k - 1)(\eta_k - \eta_{bk}) = 0, \quad \eta_k = \bar{0}, \bar{1}, \quad (7)$$

$$\frac{\partial^2 G}{\partial \eta_k^2} \leq 0, \quad \eta_k = \bar{0} \quad (A \rightarrow M_k) \quad (8)$$

$$\frac{\partial^2 G}{\partial \eta_k^2} \leq 0, \quad \eta_k = \bar{1} \quad (M_k \rightarrow A). \quad (9)$$

The transformation energy associated with $A \leftrightarrow M_k$ is

$$G(\boldsymbol{\sigma}, \theta, \bar{0}) - G(\boldsymbol{\sigma}, \theta, \bar{1}) = \boldsymbol{\sigma} : \boldsymbol{\varepsilon}_{tk} - \Delta G^\theta. \quad (10)$$

Combining Eqs. (7) and (10) with similar steps described in Sec. II and discussed in detail in [12], we get

$$\begin{aligned} \eta_{bk} = & -6\boldsymbol{\sigma} : \boldsymbol{\varepsilon}_{tk} - 6\boldsymbol{\sigma} : (\boldsymbol{\lambda}_k - \boldsymbol{\lambda}_0) : \boldsymbol{\sigma}/2 \\ & - 6\boldsymbol{\sigma} : (\boldsymbol{\varepsilon}_{\theta k} - \boldsymbol{\varepsilon}_{\theta 0}) + 6\Delta G^\theta + 1/2. \end{aligned} \quad (11)$$

Following the steps given in [14], we arrive at the symmetry preserving polynomial structure of the interaction potential

$$\begin{aligned} F_{ij} = & \eta_i \eta_j (1 - \eta_i - \eta_j) [B \{(\eta_i - \eta_j)^2 - \eta_i - \eta_j\} \\ & + D\eta_i \eta_j] + \eta_i^2 \eta_j^2 (\eta_i Z_{ij} + \eta_j Z_{ji}), \end{aligned} \quad (12)$$

where B , D are constants to be estimated from experiments. The transformation energy associated with $M_i \rightarrow M_j$ is already satisfied in this approach. Finally, the uniqueness of multi-variant PT at a material point is now imposed, which leads to

$$\begin{aligned} \frac{\partial}{\partial \boldsymbol{\sigma}} \left[\sum_{k=1}^2 \sum_{j=k+1}^3 \frac{\partial F_{kj}(\eta_k, \eta_j)}{\partial \eta_k} \right] = & \sum_{k=1}^3 \left[\boldsymbol{\varepsilon}_{tk} \frac{\partial \varphi(\eta_k)}{\partial \eta_k} \right. \\ & \left. + (\boldsymbol{\varepsilon}_{\theta k} - \boldsymbol{\varepsilon}_{\theta 0}) \frac{\partial \varphi(\eta_k)}{\partial \eta_k} + (\boldsymbol{\lambda}_k - \boldsymbol{\lambda}_0) \frac{\partial \varphi(\eta_k)}{\partial \eta_k} \boldsymbol{\sigma} \right]. \end{aligned} \quad (13)$$

The constants Z_{ij} can be estimated with the help of Eq. (13).

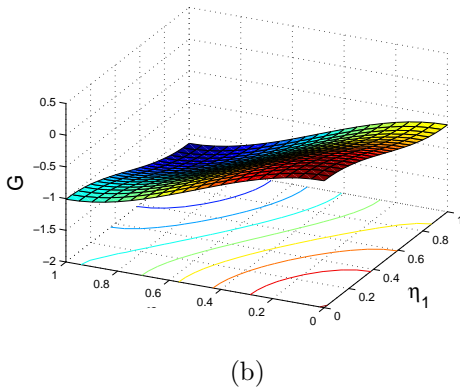
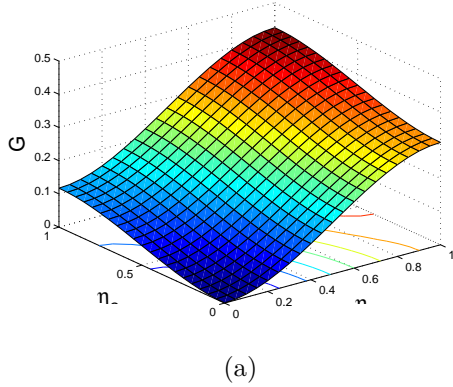


Fig. 1. Variation of Gibbs free energy (plotted in 10^8 scale) at various diffused state (η_1, η_2) during stress induced transformation, $\theta_e = 215K$, $\theta = 300K$, (a) $\sigma = 100MPa$ (b) $\sigma = 200MPa$.

For numerical illustration of the Gibbs free energy function derived above, we consider NiAl with two martensitic variants. Equal deviation of critical temperature from equilibrium temperature is assumed. The internal energy is assumed to be proportional to the difference between temperature and the equilibrium temperature in the close neighborhood of the transformation [14]. Fig. 1(a) and (b) respectively shows the distribution of the Gibbs free energy under applied stress of $100MPa$ and $200MPa$. With the help of the stress-strain curves (not shown here), it is observed that loading upto $100MPa$ and $300K$ does not produce phase transformation. As a result, G is minimum at $\eta_1 = 0$, $\eta_2 = 0$. On the other hand, martensites have already formed for loading up to $200MPa$ ($300K$), which shows global minimum at $\eta_1 = 1$, $\eta_2 = 1$. We now turn our attention to the transformation kinetics.

IV. PHASE TRANSFORMATION KINETICS COUPLED WITH THERMOELASTICITY

Our objective is to solve the coupled field model in which the phase transformation kinetics is governed by the Ginzburg-Landau equation

$$\frac{\partial \eta_k}{\partial t} = - \sum_{p=1}^3 L_{kp} \left[\frac{\partial G}{\partial \eta_p} + \beta_p : \nabla \nabla \eta_p \right] + \theta_k, \quad (14)$$

where L_{kp} are positive definite kinetic coefficients, β_p are positive definite second rank tensor, θ_k is the thermal fluctuation satisfying the dissipation-fluctuation theorem arising in context of non-equilibrium thermodynamics. While Eq. (14) governs the evolution process, the macroscopic energy conservation law is governed by the heat conduction equation

$$\rho \frac{\partial \bar{G}}{\partial t} - \boldsymbol{\sigma} : \nabla \frac{\partial \mathbf{u}}{\partial t} + \nabla \cdot \mathbf{q} = h_\theta, \quad (15)$$

and the momentum balance equation

$$\rho \frac{\partial^2 \mathbf{u}}{\partial t^2} = \nabla \cdot \boldsymbol{\sigma} + \mathbf{p}, \quad (16)$$

where

$$\bar{G} = G - \theta \frac{\partial G}{\partial \theta} \quad (17)$$

is the internal energy, ρ is the mass density, \mathbf{u} is the displacement vector,

$$\mathbf{q} = -\kappa \nabla \theta - \alpha' \kappa \nabla \frac{\partial \theta}{\partial t} \quad (18)$$

is the heat flux approximated from the solution of 3D Cattaneo-Vernotte equation [6], h_θ and \mathbf{p} are the thermal loading and body force, respectively. The displacement is related to the Green strain tensor as

$$\boldsymbol{\varepsilon} = \frac{1}{2} [\mathbf{F} : \mathbf{F} - \mathbf{I}], \quad (19)$$

where \mathbf{F} is the deformation gradient and \mathbf{I} is the identity tensor. Thus, in a quasi-static sense, the framework described here requires the minimization of the total

energy[1, 21]

$$\int_{\Omega} G(\nabla \mathbf{u}(\mathbf{x}), \theta) d\mathbf{x} + \text{loading device energy}, \quad (20)$$

expressed in the deformed configuration of the lattice. Note also that in our model, the order parameters η_k , which appears in the stress in Eq. (20), provides the important connection between the transformation of the lattice vector and the continuum elasticity. Further, in order to model the evolution process, one requires a variational formulation involving a suitable weak form of the Initial Boundary Value Problem (IBVP). This is discussed in the following section where we develop a three-dimensional finite element model of the IBVP.

V. FINITE ELEMENT FORMULATION

We derive the weak form of the coupled nonlinear system (Eqs. (14)-(16)) using weighted residual approach. We interpolate the fields $\mathbf{u}(x, y, z, t)$, $\theta(x, y, z, t)$ and $\eta_k(x, y, x, t)$ ($k = 1, \dots, n$) using non-conforming finite element, with h -refinement. This is an established scheme for modeling SMA microstructure [18]. Noting that all the three governing equations have highest order of spatial derivative as two, we choose the standard Lagrangian isoparametric interpolation function \mathbf{N} ,

$$\{u_1 \ u_2 \ u_3\}^T = \mathbf{N}_u \mathbf{v}^e, \quad \theta = \mathbf{N}_\theta \mathbf{v}^e, \quad \eta = \mathbf{N}_\eta \mathbf{v}^e, \quad (21)$$

$$\mathbf{v} = \{u_1 \ u_2 \ u_3 \ \theta \ \eta_1, \dots, \eta_n\}^T. \quad (22)$$

Here, the superscript e indicates element nodal quantities. Introducing admissible weights ($\bar{u}_i, \bar{\theta}, \bar{\eta}_k$) chosen from the linear span of \mathbf{v}^e , a variational statement can be posed as

$$\delta \Pi = \delta \Pi_{PT} + \delta \Pi_\theta + \delta \Pi_u + \delta W = 0, \quad t \in [0, +\infty] \quad (23)$$

where

$$\begin{aligned} \Pi_{PT} &= \int_{\Omega} \sum_{k=1}^n \bar{\eta}_k \left[\frac{\partial \eta_k}{\partial t} - \theta_k \right] d\mathbf{x} \\ &+ \int_{\Omega} \sum_{k=1}^n \sum_{p=1}^n \bar{\eta}_k \left[L_{kp} \left(\frac{\partial G}{\partial \eta_p} + \beta_p : \nabla \nabla \eta_p \right) \right] d\mathbf{x}, \end{aligned} \quad (24)$$

$$\begin{aligned} \Pi_\theta &= \int_{\Omega} \bar{\theta} \left[\rho \frac{\partial \bar{\theta}}{\partial t} - \boldsymbol{\sigma} : \nabla \frac{\partial \mathbf{u}}{\partial t} \right] d\mathbf{x} \\ &+ \int_{\Omega} \bar{\theta} \left[\nabla \cdot \left(-\kappa \nabla \theta - \alpha' \kappa \nabla \frac{\partial \theta}{\partial t} \right) - h_\theta \right] d\mathbf{x}, \end{aligned} \quad (25)$$

$$\Pi_u = \int_{t_1}^{t_2} \int_{\Omega} \bar{\mathbf{u}} \left[\rho \frac{\partial^2 \mathbf{u}}{\partial t^2} - \nabla \cdot \boldsymbol{\sigma} - \mathbf{p} \right] d\mathbf{x}, \quad (26)$$

and W is the external work done. Integrating Eqs. (21)-(23) by parts and applying divergence theorem, we get the discrete nonlinear finite element model, which can be expressed in matrix notations as

$$\begin{aligned} \{\delta \mathbf{u}\}^e : & \int_{\Omega} [\mathbf{N}_u]^T \rho [\mathbf{N}_u] \{\ddot{\mathbf{v}}\}^e + \int_{\Omega} [\mathbf{B}_u]^T \{\boldsymbol{\sigma}\} \\ &= \int_{\Gamma} [\mathbf{N}_u]^T \{\mathbf{p}\} + \{\mathbf{f}\}^e, \end{aligned} \quad (27)$$

$$\begin{aligned} \{\delta \theta\}^e : & \int_{\Omega} [\mathbf{N}_\theta]^T \rho [\dot{\mathbf{G}}'] \{\mathbf{v}\}^e + \int_{\Omega} [\mathbf{N}_\theta]^T \rho [\mathbf{G}'] \{\dot{\mathbf{v}}\}^e \\ &- \int_{\Omega} [\mathbf{N}_\theta]^T \rho [\mathbf{N}_\theta] \{\mathbf{v}\}^e \left([\nabla_\theta \dot{\mathbf{G}}'] \{\mathbf{v}\}^e + [\nabla_\theta \mathbf{G}'] \{\dot{\mathbf{v}}\}^e \right) \\ &+ \int_{\Omega} [\mathbf{N}_\theta]^T \{\boldsymbol{\sigma}\}^T [\nabla \mathbf{N}_u] \{\mathbf{v}\}^e + \int_{\Omega} [\mathbf{B}_\theta]^T \kappa [\mathbf{B}_\theta] \{\mathbf{v}\}^e \\ &+ \int_{\Omega} [\mathbf{B}_\theta]^T \alpha' \kappa [\mathbf{B}_\theta] \{\dot{\mathbf{v}}\}^e = \int_{\Gamma} [\mathbf{N}_\theta]^T \{\mathbf{q}_\theta\}^e, \end{aligned} \quad (28)$$

$$\begin{aligned} \{\delta \eta\} : & \int_{\Omega} [\mathbf{N}_\eta]^T [\mathbf{N}_\eta] \{\dot{\mathbf{v}}\}^e + \int_{\Omega} [\mathbf{N}_\eta]^T [\mathbf{L}] [\mathbf{G}''] [\mathbf{N}_\eta] \{\mathbf{v}\}^e \\ &- \int_{\Omega} [\nabla \mathbf{N}_\eta]^T [\mathbf{L}] [\boldsymbol{\beta}] [\nabla \mathbf{N}_\eta] \{\mathbf{v}\}^e + \int_{\Gamma} [\mathbf{N}_\eta]^T [\mathbf{L}] [\boldsymbol{\beta}] [\nabla \mathbf{N}_\eta] \{\mathbf{v}\}^e \\ &= \int_{\Gamma} [\mathbf{N}_\eta]^T \{\theta_k\}^e, \end{aligned}$$

where $[\mathbf{B}_u]$ is the strain-displacement matrix and $[\mathbf{B}_\theta]$ is its thermal analog. The stress vector is expressed as

$$\begin{aligned} \{\boldsymbol{\sigma}\} &= [\mathbf{C}(\eta_k)] [\mathbf{B}_u] \{\mathbf{v}\}^e - [\mathbf{C}^t(\eta_k, \boldsymbol{\varepsilon}_{tk})] [\mathbf{N}_\eta] \{\mathbf{v}\}^e \\ &- [\mathbf{C}^\alpha(\eta_k, \alpha_0, \alpha_k)] [\mathbf{N}_\theta] (\{\mathbf{v}\}^e - [\mathbf{I}] \{\theta_e\}), \end{aligned} \quad (29)$$

where the elastic stiffness including the phase inhomogeneity is

$$[\mathbf{C}(\eta_k)] = \left[[\boldsymbol{\lambda}_0] + \sum_k ([\boldsymbol{\lambda}_k] - [\boldsymbol{\lambda}_0]) \varphi(\eta_k) \right]^{-1}, \quad (30)$$

the transformation-induced stress coefficient matrix is

$$[\mathbf{C}^t(\eta_k, \boldsymbol{\varepsilon}_{tk})] = [\mathbf{C}(\eta_k)] \sum_k \{\boldsymbol{\varepsilon}_{tk}\} \bar{\varphi}(\eta_k), \quad (31)$$

$$\bar{\varphi}_k = (\varphi_k / \eta_k, 0) \quad |\eta_k| \geq 0, \quad (32)$$

and the temperature-induced stress coefficient matrix including the phase inhomogeneity is

$$[\mathbf{C}^\alpha(\eta_k, \alpha_0, \alpha_k)] = [\mathbf{C}(\eta_k)] \left([\alpha_0] + \sum_k ([\alpha_k] - [\alpha_0]) \varphi(\eta_k) \right). \quad (33)$$

The nonlinear terms are decomposed as

$$G = \sum_k (\bar{G}_k + \bar{F}_k) \eta_k = ([\bar{G}] + [\bar{F}]) [\mathbf{N}_\eta] \{\mathbf{v}\}^e = [\mathbf{G}'] \{\mathbf{v}\}^e, \quad (34)$$

$$\left\{ \frac{\partial G}{\partial \eta_p} \right\} = [\tilde{\mathbf{G}}] \{\eta\} = [\mathbf{G}''] \{\mathbf{v}\}^e. \quad (35)$$

In Eq. (27), $\{\mathbf{f}\}^e$ is the nodal force vector. In Eq. (28), $\{\mathbf{q}_\theta\}^e$ is the thermal flux vector. Considering the effect of ambient environment surrounding the SMA sample, the total thermal flux normal to the material surface (Γ) is defined as $q_\theta = q_0 - h_c(\theta - \theta_0)$, where q_0 is the externally applied flux, θ_0 is the ambient temperature and h_c is the associated convection coefficient.

A. Numerical implementation

We implemented the finite element model described by Eqs. (27)-(29) with the associated Dirichlet boundary conditions and the initial conditions in a general three-dimensional finite element code. For the present problem we use 8-node, 7 d.o.f./node tetrahedral element with tri-linear isoparametric interpolation and reduced Gauss-quadrature integration for shear terms. We employed Newmark's time integration scheme. The analysis of numerical stability for such a strongly coupled problem is not a trivial task and is currently under our scrutiny. Note that in the context of viscoplasticity, the stability issues for the approximation based on a generalized mid-point rule (first-order accurate) has been discussed in [22], and an extension of such an analysis to higher-order schemes may be needed for the present problem. The main difficulty, specific to the problem, lies with the fact that the solid-state transformation process is spontaneous in nature and the associated rates vary over a wide range as compared to continuum elasto-plasticity.

This brings to further difficulties in organizing nonlinear iterations. Note that the energy minimization process can take a different and unphysical path unless the phase transformation conditions in Eqs. (8)-(9) are enforced in a consistent manner in the incremental algorithm. We base our algorithm on the following steps:

1. With the known matrices and vectors obtained from the time step $t = t_i$, compute the stress and transformation barrier.
2. Check the loss of stability $A \leftrightarrow M_k \forall k$. Obtain the increment $\Delta\eta_k$ by satisfying consistency condition in the neighborhood of the transformation surface (similar to the return mapping algorithm for elasto-plasticity [22]).
3. Compute the consistent tangent matrix $[\mathbf{K}]_t$. Here the effective internal force vector has three parts:

$$\{\mathbf{b}\} = \left\{ \{\mathbf{f}\}_u^T \{\mathbf{f}\}_\theta^T \{\mathbf{f}\}_\eta^T \right\}^T,$$

$$\mathbf{f}_u = -\frac{\partial \Pi_u}{\partial \mathbf{u}}, \mathbf{f}_\theta = -\frac{\partial \Pi_\theta}{\partial \theta}, \mathbf{f}_\eta = -\frac{\partial \Pi_{PT}}{\partial \eta_k}.$$

The incremental update at n th iteration is obtained as

$$\{\Delta \mathbf{v}\}_{n+1}^e = -[\mathbf{K}]_t^{-1} (\{\mathbf{b}\}_{n+1}^{\text{int}} - \{\mathbf{b}\}_{n+1}^{\text{ext}}), \quad (36)$$

$$[\mathbf{K}]_t = \bigcup_e \frac{\partial \mathbf{b}}{\partial \mathbf{v}^e},$$

4. Eq. (36) is then solved by Newton's iterations until a specified accuracy is achieved.
5. Compute the updated vectors, velocity and acceleration and move to next time step $t_{i+1} = t_i + \Delta t$.

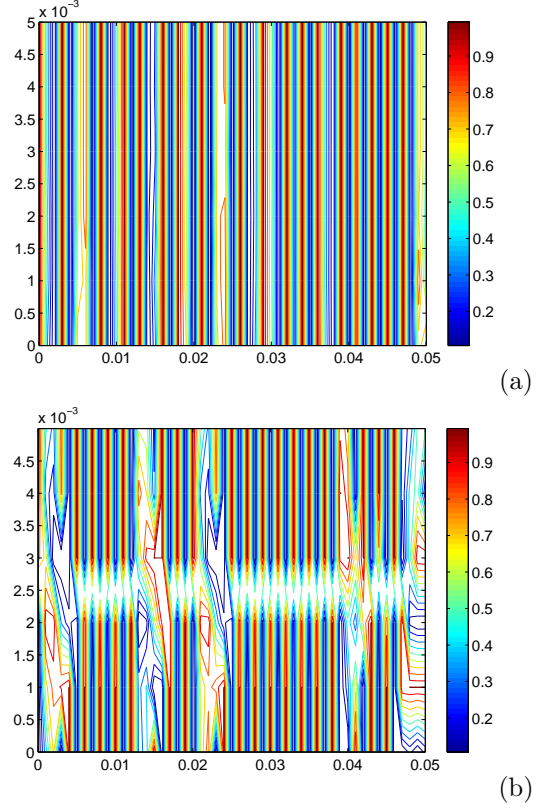


Fig. 2. Evolution of (a) η_1 and (b) η_2 . Both snapshots are presented at $t = 0.5ms$.

VI. NUMERICAL SIMULATION

Numerical simulation of $A \rightarrow M_k$ is reported in this paper by considering a $50mm \times 5mm \times 100\mu m$ Ni-Al film under in-plane stress pulse. The film is assumed to be restrained at the edge $x = 0$ and subjected to in-plane longitudinal stress along the edge $x = 50mm$. The surfaces are assumed to be in ambient environment ($\theta = 298K$). The applied stress history is a typical Gaussian distribution with effective range of approximately $0.5ms$, peak stress at approximately $0.1ms$. The peak stress is taken as $1600MPa$ such that the initial state of pure austenite is transformed into martensites as the stress wave propagates from $x = 50mm$ towards $x = 0$. The film has been discretized using $50 \times 5 \times 1$ elements with finite element system size of 612. Uniform mesh has been used, although future studies are needed with more refined meshes and appropriate mesh transformation scheme to physically represent the microstructural compatibility. Uniform time step of $\Delta t = 5\mu s$ has been used. We observe that as the stress attains its peak at $x = 50mm$, $t = 0.1ms$, the spatial patterns of both η_1 and η_2 are fairly diffused. These patterns are then evolved into arrays typical for martensites, as demonstrated in Figs. 2. Such structures with alternating bands of martensites resemble those observed in time-resolved microscopy of SMA films. In particular, a needle like pattern can be seen in Fig. 2. Similar structures have been studied before, e.g. in [11]. Our preliminary numerical studies based on the newly developed nonlinear coupled finite element model

correspond to usually observed microstructures previously reported. A comprehensive set of simulation studies is currently under progress. Through such simulations, it should be possible to gain a better understanding of complex evolution of the multivariant phases and thermomechanical processing of SMA samples for engineering applications.

VII. CONCLUSIONS

A three-dimensional thermo-elastically coupled nonlinear dynamic finite element model for phase transformations in SMA has been developed. Computational implementation of the model has been discussed in detail. A special attention has been given to the study of phase transformation kinetics in a NiAl thin film under transient in-plane stress. It has been shown that the numerical simulation captures the essential features of the evolved textures such as array of martensitic bands and needle shaped twinned layers at the interfaces.

REFERENCES

- [1] J.M. Ball and C. Cartensen, "Compatibility conditions for microstructures and the austenite-martensite transition," *Material Science and Engineering A*, Vol.273-275, pp. 231-236, 1999.
- [2] P. Belik and M. Luskin, "A computational model for the indentation and phase transition of a martensitic thin film," *J. Mech. Phys. Solids*, Vol. 50, pp. 1789-1815, 2002.
- [3] M. Brocca, L.C. Brinson and Z.P. Bazant, "Three-dimensional constitutive shape memory alloys based on microplane model," *J. Mech. Phys. Solids*, Vol. 50, pp. 1051-1077, 2002.
- [4] V.I. Levitas and D.L. Preston, "Three-dimensional Landau theory for multivariant stress-induced martensitic phase transformations. III. Alternative potentials, critical nuclei, kink solutions, and dislocation theory," *Physical Rev. B*, Vol. 68, p.134201, 2003.
- [5] A. Berezovski and G.A. Maugin, "Simulation of wave and front propagation in thermoelastic materials with phase transformation," *Computational Materials Science*, Vol.28, pp. 478-485, 2003.
- [6] R.V.N. Melnik, A.J. Roberts and K.A. Thomas, "Computing dynamics of copper-based shape memory alloys via center manifold reduction of 3D models," *Computational Materials Science*, Vol. 18, pp. 255-268, 2000.
- [7] P.K. Purohit and K. Bhattacharya, "Dynamics of strings made of phase-transforming materials," *J. Mech. Phys. Solids*, Vol. 51, pp. 393-424, 2003.
- [8] F. Falk and P. Konopka, "Three-dimensional Landau theory describing the martensitic phase transformation of shape-memory alloys," *J. Phys.: Condens. Matter*, Vol. 2, pp. 61-77, 1990.
- [9] R. Abeyaratne, C. Chu and R.D. James, "Kinetics of materials with wiggly energies: The evolution of twinning microstructure in a Cu-Al-Ni shape memory alloys," *Phil. Mag.*, Vol. 73A, pp. 457-496, 1996.
- [10] D. Schryvers and D.H. Moritz, "Martensitic transformations and microstructures in splat-cooled Ni-Al," *Material Science and Engineering A*, Vol. 273-275, pp. 697-702, 1999.
- [11] B. Li and M. Luskin, "Theory and computation for the microstructure near the interface between twinned layers and a pure variant of martensite," *Material Science Engineering A*, Vol. 273-275, pp. 237-240, 1999.
- [12] D.R. Mahapatra and R.V.N. Melnik, "A dynamic model for phase transformations in 3D samples of shape memory alloys," *LNCS Springer-Verlag*, Vol. 3516, pp.25-32, 2005.
- [13] V.I. Levitas and D.L. Preston, "Three-dimensional Landau theory for multivariant stress-induced martensitic phase transformations. I. Austenite \leftrightarrow martensite," *Physical Rev. B*, Vol. 66, p.134206, 2002.
- [14] V.I. Levitas and D.L. Preston, "Three-dimensional Landau theory for multivariant stress-induced martensitic phase transformations. II. Multivariant phase transformations and stress space analysis," *Physical Rev. B*, Vol. 66, p.134207, 2002.
- [15] T. Ichitsubo, K. Tanaka, M. Koiwa and Y. Yamazaki, "Kinetics of cubic to tetragonal transformation under external field by the time-dependent Ginzburg-Landau approach," *Phy. Rev. B*, Vol. 62, p.5435, 2000.
- [16] J.G. Boyd and D.C. Lagoudas, "A thermodynamical constitutive constitutive model for shape memory materials. Part I. the monolithic shape memory alloy," *Int. J. Plasticity*, Vol. 12(6), pp.805-842, 1996.
- [17] X. Wu, D.S. Grummon, T.J. Pence, "Modeling phase fraction shakedown during thermomechanical cycling of shape memory materials," *Materials Science Engineering A*, Vol. 273-275, pp. 245-250, 1999.
- [18] B. Li and M. Luskin, "Finite element analysis of microstructure for the cubic to tetragonal transformation," *SIAM J. Numer. Anal.*, Vol.35, pp. 376-392, 1998.
- [19] P. Matus, R.V.N. Melnik, L. Wang and I. Rybak, "Application of fully conservative schemes in nonlinear thermoelasticity: modelling shape memory materials," *Mathematics and Computers in Simulation*, Vol. 65, pp. 489-510, 2004.
- [20] S. Fu, S., Y. Huo, and I. Muller, "Thermodynamics of pseudoelectricity - an analytical approach," *Acta Mechanica*, Vol. 99, pp. 1-19, 1991,
- [21] R.D. James and K.F. Hane, "Martensitic transformations and shape memory materials," *Acta Materialia*, Vol. 48, pp.197-222, 2000.
- [22] J.C. Simo and T.J.R. Hughes, "Computational Inelasticity," Springer-Verlag, 1997.

CONTENTS

1. Control of Complex Systems Subject to Information Structure Constraints: A Brief Review and New Results.....	(1)
D. D. Šiljak, A. I. Zečević	
2. Combat Decision Support Subsystem for Optimal Weapon-Target Assignment.....	(11)
Z. R. Bogdanowicz, N. P. Coleman, S. J. Kaniyantethu	
3. Ship Steering Intelligent Control Based on Adaptive Heuristic Critic Algorithm.....	(16)
Zhipeng Shen, Chen Guo	
4. Design and Implementation of High-Speed Parallel ATR System.....	(21)
Guangzhou Zhao, Tianxu Zhang, Zhiguo Cao	
5. Functional Procedure Neural Network.....	(27)
Jiuzhen Liang	
6. Brittleness analysis of Electric Network.....	(32)
Hongzhang Jin, Limei Yan, Panxiang Rong, Xiaobin Liu, Mengda Li	
7. Nonlinear Adaptive Fuzzy Control for Ship Steering.....	(37)
Shichun Yuan, Chen Guo, Yansheng Yang	
8. Fuzzy Variable Structure Control for Chaotic systems.....	(43)
Hong Gu, Hongwei Wang, Zhelong Wang	
9. Study on Fault Diagnosis for Engineering System Based on Multi-Agents.....	(47)
Daqi Zhu, Wuzhao Li	
10. Qualitative Analysis and Quantified Evaluation of Information Fusion Efficiency in Multi-sensor Systems.....	(52)
Lizhong Xu, Zhigui Lin, Simon X. Yang	
11. Design Study of a Pipe Profile Detector.....	(57)
Hong Gu, Zhelong Wang, Hongwei Wang, Min Wang	
12. Robust Backstepping Control of Flexible-Link Manipulators using Neural Networks.....	(62)
Yuangang Tang, Fuchun Sun, Zengqi Sun	
13. A Mining Algorithm FTDA2 with Reduced Computed Time.....	(67)
Zengjin Qian, Shiguang Ju, Yan Xin, Hong Yang	
14. Chaos in the Quasiperiodically Excited Softening Duffing Oscillator with Nonlinear Damping	(73)
Jingjun Lou, Shijian Zhu, Shuyong Liu	
15. Fuzzy Wavelet Support Vector Machines and Its Application in modeling Jet Fuel Endpoint	

- 102. Parametric Study on the Stability of a 2-D Supersonic Lifting Surface with Time Delayed Linear and Nonlinear Feedback Controls.....(535)**
Zhen Chen, Pei Yu
- 103. Interband-Resonant-Tunneling-Diode (I-RTD) Vertical-Cavity Laser.....(541)**
Boris Gelmont, Dwight Woolard
- 104. A Bound Method for a Class of Nonlinear Discrete Optimum Design.....(547)**
L. S. Shi, Q. G. Meng, Z. C. Xuan
- 105. Neuro-Fuzzy Adaptive Control for Flexible-link Robots Including Motor Dynamics.....(551)**
Fuchun Sun, Hao Wu, Huaping Liu
- 106. Three-dimensional Mathematical Models of Phase Transformation Kinetics in Shape Memory Alloys.....(557)**
D. Roy Mahapatra, R. V. N. Melnik
- 107. Simple Two-Input Two-Output Takagi-Sugeno Fuzzy Controllers of PI or PD Type.....(563)**
Hao Ying
- 108. Oscillation of Nonlinear Impulsive Delay Hyperbolic Equation with Application to Hyperbolic Heat Conduction.....(568)**
Anping Liu, Deyi Xu, Yunan Li, Liu Ting
- 109. Stability Switches of a Controlled van der Pol-Duffing Oscillator.....(574)**
J. C. Ji, C. C. Lim, C. H. Hansen
- 110. Feedback Control of TCP Flows in Computer Network using Random Early Discard (RED) Mechanism.....(578)**
N. U. Ahmed, Cheng Li
- 111. Macroscopic Curvature-based Fingerprint Feature Extraction and Analysis.....(584)**
Youjun Xu, Simon X. Yang, Guiming He, Xiong Zhang
- 112. Application of Intelligent Self-tuning PID in Speed Control System of BLDC and Realization of DSP.....(590)**
Yong Chen, Xiyue Huang
- 113. Asymptotic Stability Results for Large Scale Nonlinear Discrete-Time Delay Systems.....(596)**
S. Sathananathan, O. Adetona, L. H. Keel
- 114. Control Parametrization Enhancing Transform for Optimal Impulsive Control Problems.....(602)**
K. L. Teo, R. Li, V. Rehbock, Y. Liu
- 115. Preferential Multi-Objective Genetic Algorithm for JPEG Quantization Table Optimization.....(608)**
Hanli Wang, Sam Kwong